Wear resistance of blades in planetary concrete mixers. Design of a new improved blade shape and 2D validation

Maria Cristina Valigi[a], Silvia Logozzo[a], Mirko Rinchi[b]

[a] Department of Engineering – University of Perugia – Via G. Duranti, 1 – 06125 Perugia (Italy)
[b] Department of Industrial Engineering – University of Florence – Via Santa Marta, 3 – 50139 Firenze (Italy)

Maria Cristina Valigi – Associate Professor – Corresponding Author – Via G. Duranti 1, 06125 Perugia (Italy) – e-mail: mariacristina.valigi@unipg.it

Silvia Logozzo – silvia.logozzo@unipg.it
Mirko Rinchi – mirko.rinchi@unifi.it

Abstract

Wear of machine components is one of the main phenomena to control and limit in order to improve the performance and reduce the production costs. In this paper, the optimization of a planetary concrete mixer in terms of wear resistance of blades is proposed and a new design of the mixing blades' shape is shown and discussed. Experimental tests performed with two stars planetary concrete mixers are described and achieved experimental results are shown. Those results display the progress of blades' wear over time and prove that the proposed modified blade's geometry improves the wear resistance and extends the useful-life.

Keywords:

Planetary concrete mixer

Wear resistance

Mixing blades

Bingham fluid

1. Introduction

Performance optimization of a concrete mixer is an issue of great significance in many industrial technologies and wear is one of the main phenomena to forecast and test during the design and working of mechanical components. The wear effect is the progressive modification of surfaces' morphology that brings the mechanical components to inefficiency.

An overview of the various types of mixing methods and concrete mixers commercially available are described in [1–5].

In the present paper, a planetary concrete mixer is studied and the wear resistance of mixing blades is investigated. The analysis of the concrete mixer is based on the forces exchanged among mixing arms, blades and concrete.

Only a few published articles present experimental and theoretical researches about planetary concrete mixers. For instance, Cazacliu and Legrand [6] present the results of tests on planetary concrete mixers and investigate the correlation between the paste composition and the power necessary for the mixing operation. Cazacliu [7] presents a model of the power consumption as a function of the planetary motion.

Braccesi et al. [8] show that the Brinch-Hansen formula [9] and the Bingham theory of fluids [10–12] can be used to describe the behavior of concrete in the so-called dry and final mixing phases. A calculation of blades' forces resulting from the application of a model is proposed in [13] and [14] in order to evaluate the useful life of the gear units of the planetary concrete mixer. Some mixing performances are analyzed by Yao et al. [15]. Relationships between mixing methods and both rheological properties and microstructure of cement pastes are described in [16].

Since the mixing blades suffer wear more than other components, they are designed to be easily replaced in all the concrete mixers' types. However, their decay is low and slow when they undergo the proper maintenance program.

In this paper, the authors present the study of wear of mixing blades used in planetary concrete mixers and propose a new improved blade design allowing longer durability.

The machine and the mixing process are described, together with the models presented in literature, in order to characterize the process. The main factors influencing wear of blades are: kinematics, friction between slurry and blades, friction due to the leakage between vessel and blades and also an inadequate maintenance of the mixer.
The authors will examine the wear behavior of some prototypes of the proposed new blades by comparing the experimental data obtained in a concrete batching plant during typical production days.

2. Description of planetary concrete mixers and mixing cycle

Planetary concrete mixers are highly suitable for experimental studies because they guarantee the homogeneity of the mixture and the repeatability of the tests.
Planetary concrete mixers are mainly divided into two categories: single and double star mixers (Fig. 1). They have a vertical axis, a fixed tank and they realize a planetary motion by gear units.

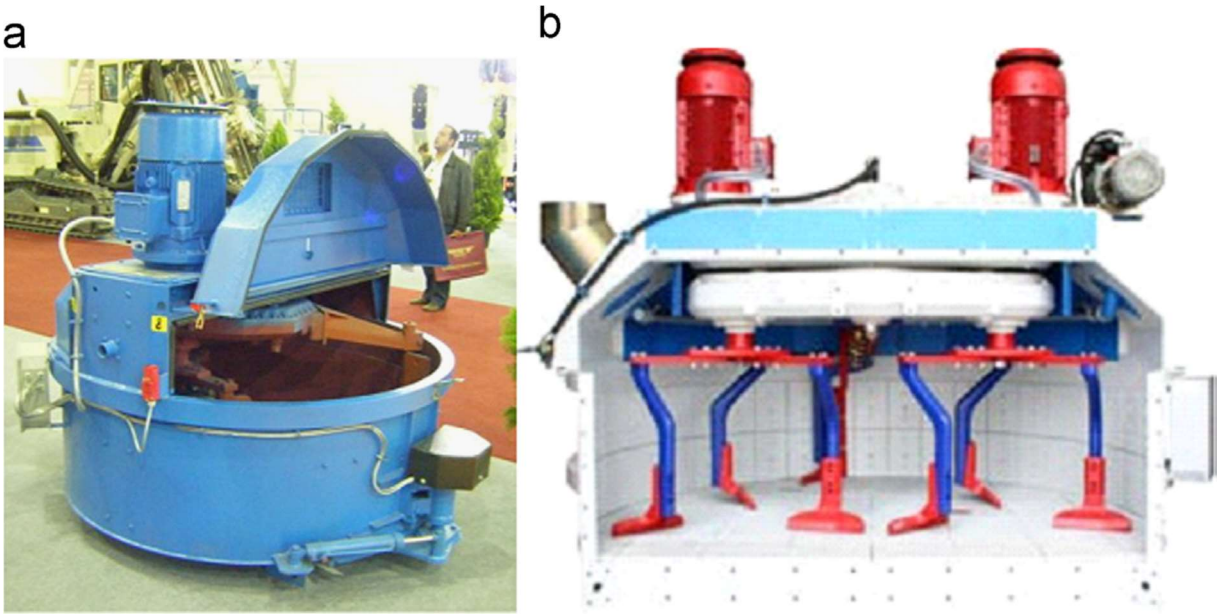

Fig. 1 Planetary concrete mixer: (a) single and (b) double star

The main components of a planetary concrete mixer are:

- Electric motors: there is one motor for each star, 1 to 3 depending on the tank's size.
- The gear box: it contains two mechanisms, one is the ordinaryreduction gear train and one is the planetary gear train which transmits the planetary motion from the motors to the stars.

- Stars and mixing arms: each star includes three arms, whichare the main components in charge of the mixing function. The mixing arms are peripheral and obtained by steel drill rods.
- Mixing blades: although their name would suggest that theblades are in charge of the mixing procedure, their main function is the discharge operation and their presence does not influence the homogeneity of the final mixture. Blades are the concrete mixer's components mostly interested by wear.
- Mixing tank with the swing-out doors: the mixing bladescarry out the discharge operation throughout swing-out sector doors, sealed in rubber and hydraulically powered. Mixing arms can reach each point of the tank bottom. The mixing tank is made by extremely thick steel sheets. The entire tank is protected by a case to prevent dust escaping.

The composition of gear rotation and revolution movements of arms generates the planetary mixing motion. Fig. 2 shows the planetary system gear boxes and corresponding kinematic schematics. The first gear box and schematic refer to single star mixers, while the second ones to double star mixers. The mixing operation will be interrupted by a micro-switch if the door at the front is opened. One or two peripheral arms work as scrapers. The slurry level has to be about one third of the tank's depth.

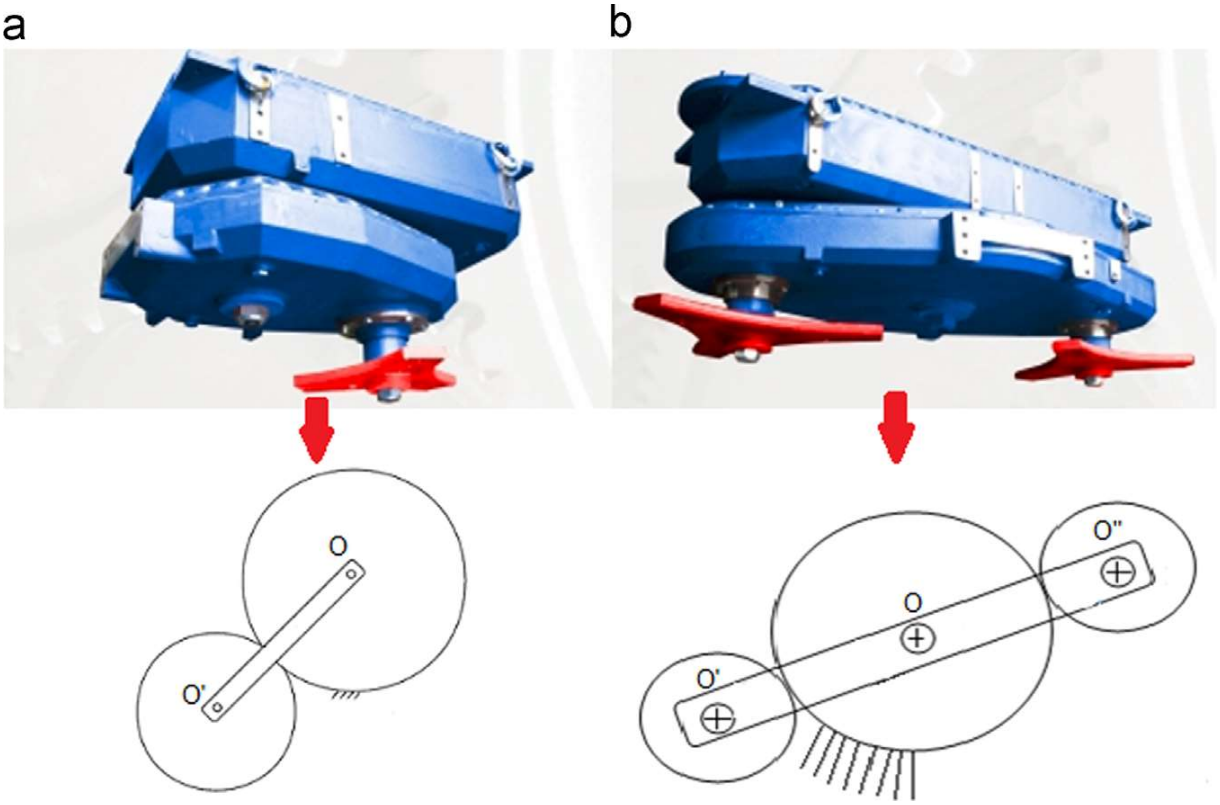

Fig. 2. Planetary system gearboxes and corresponding kinematic schematics.

Fig. 3 shows a drawing of a star in the horizontal plane. The analyzed concrete mixer has two stars and six blades (Fig. 1b).

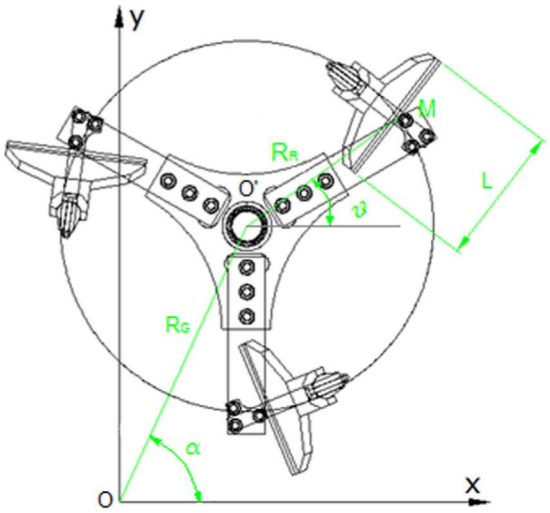

Fig. 3. Star with blades.

Fig. 4 shows the trajectories of the three arms in a single star mixer at different mixing stages [14]. As already mentioned, the mixing blades are not in charge of the mixing function and their presence does not affect the homogeneity of the mixture. This can be demonstrated also by observing Fig. 4, where it is shown how the trajectories of the mixing arms reach each position at the tank's bottom surface. In addition, according to technical reports made by customers and to the manufacturer's experience, it is known that the mixing efficiency does not change significantly during the wear progress of the mixing blades, also when the blades are at the end of their life.

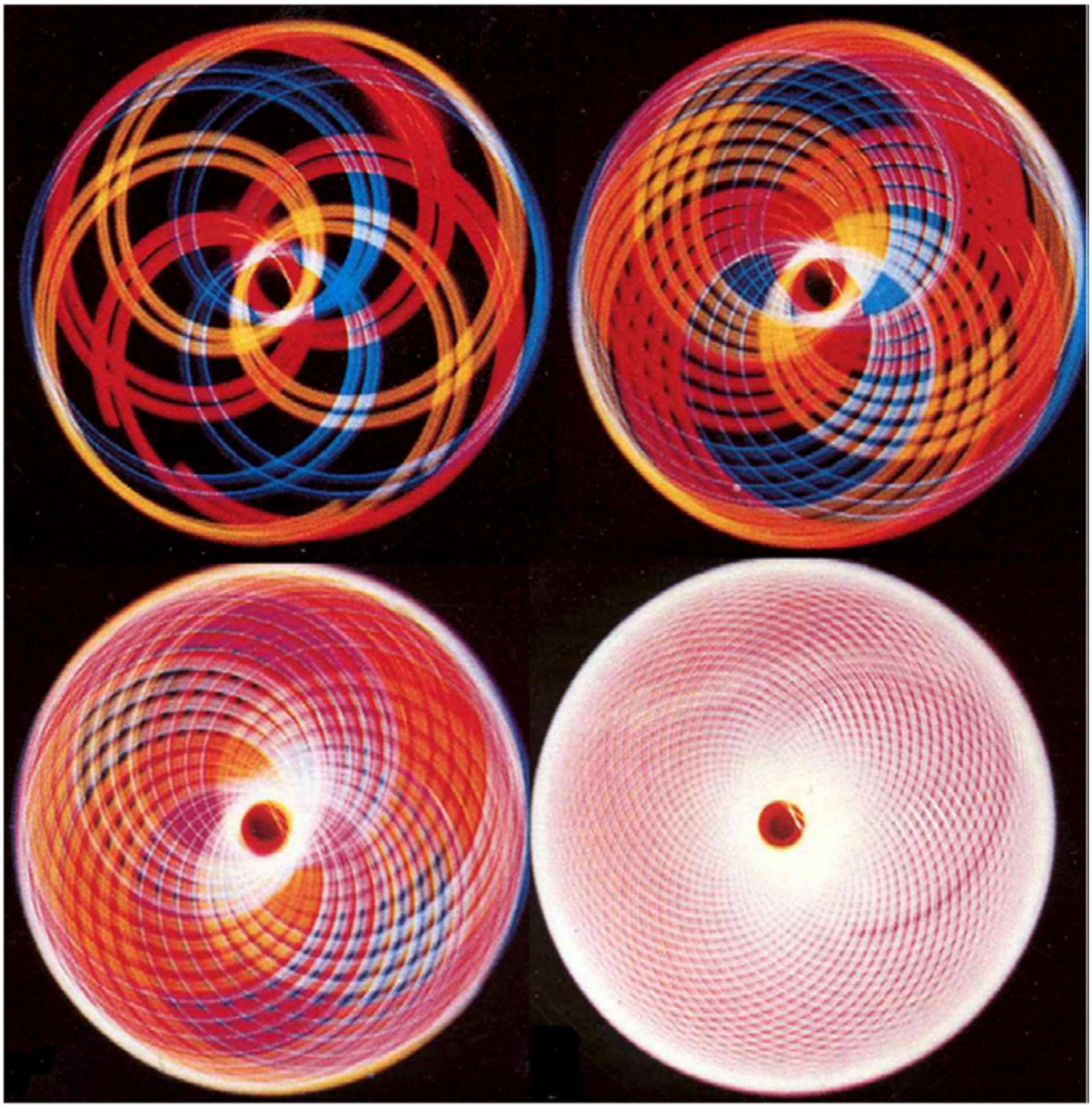

Fig. 4. Trajectories of the three arms

The phases of the mixing procedure, during a mixing cycle are:

1. Aggregates (sand) introduction
2. Cement introduction
3. Dry premixing stage
4. Water addition
5. Additives loading
6. Final mixing (regime) before discharge
7. Discharge

All the sub-mentioned phases can be highlighted in the evolution of absorbed power, during a mixing cycle. For example, Fig. 5 shows a measured evolution of absorbed power during a typical mixing cycle, in the studied two stars planetary concrete mixer. All the phases of the mixing procedure are labeled on this power consumption curve.

At the beginning of the cycle, the resistance of the paste tends to increase until the water is loaded into the mixing tank. Some seconds later, the cement paste starts to form and a lubricating action arises, thus the resistance of the mixture starts to decrease.

Therefore, the entire mixing procedure can be further divided into three macro phases:

- Dry phase: sand and cement are introduced together into themixer without water.
- Wet phase: a proper quantity of water is added to the drymixture for final mixing. During the wet phase, the physical property and behavior of the mixture change.
- Final mixing phase (regime): it starts after the water additionphase is completed. The mixer is still working for some time to allow a complete homogenization of the mixture.

Fig. 5. Measured power consumption curve and mixing phases.

In Fig. 5 one can observe that the power consumption is at its maximum value in the phase when the additives are loaded into the tank, while the regime phase is between the phase from 5 to 7. Since this is the longest phase of the mixing cycle, it can be considered as the most responsible of wear phenomena affecting blades. This is the reason why this paper is concerned with the regime phase and all the following models regard this phase.

2.1. Fresh concrete's model in the regime phase and actions on blades

During the regime phase (starting from point 6 in Fig. 5), the fresh concrete can be considered as an incompressible non-Newtonian fluid. The stress tensor for incompressible non-Newtonian fluids is given by the generalized Newtonian model:

$$\boldsymbol{\tau} = \mu^*(\dot{\gamma})\dot{\boldsymbol{\gamma}} \tag{1}$$

where $\mu^*(\dot{\gamma})$ is the apparent viscosity, $\dot{\boldsymbol{\gamma}} = \boldsymbol{\nabla u} + (\boldsymbol{\nabla u})^{\mathrm{T}}$ is the shear rate tensor and $\mathbf{u}$ is the velocity. Bold letters indicate vectors.

Various mathematical models have been suggested to describe the apparent viscosity $\mu^*(\dot{\gamma})$. When considering the Power-law model of fluid, the governing relationship for $\mu^*(\dot{\gamma})$ is:

$$\boldsymbol{\mu}^*(\dot{\boldsymbol{\gamma}}) = \mathbf{k}\,\boldsymbol{\mu}\,(\dot{\boldsymbol{\gamma}})^{(\mathbf{m-1})} \tag{2}$$

where m is the so-called power-law index and K is referred to as the consistency factor. If m is equal to 1, the Navier-Stokes constitutive equation is recovered. If m is smaller than 1, the constitutive equation is that of shear thinning whereas, if m is greater than 1, the behavior is shear thickening [17,18].

In the Carreau model the governing relationship for $\mu^*(\dot{\gamma})$ is:

$$\boldsymbol{\mu}^*(\dot{\boldsymbol{\gamma}}) = \mu_\infty + (\mu_0 - \mu_\infty)\,[1 + (\lambda\dot{\gamma})^2]^{(n-1)/2} \tag{3}$$

Where μ_∞ and μ_0 are the infinitive and zero shear viscosity respectively, λ is the molecular rotational relaxation time and n is the power-law exponent [17].

In laminar flow concrete is most often assumed to behave like a Bingham fluid. In this case, its flow is described by two parameters: limit yield stress τ_0 and plastic viscosity μ, that for the fresh concrete are $\tau_0 = 6.18$ Pa and $\mu = 6$ Pa* s. The Bingham formula is:

$$\tau = \tau_0 + \mu\dot{\gamma} = \mu^*\dot{\gamma} \tag{4}$$

where τ is the shear stress applied to the material. The apparent viscosity μ is constant, according to Eq. (2) with $m = 1$.

The forces acting on the blades during their motion are the frictional force $\mathbf{F_f}$ and the viscous force $\mathbf{F_v}$. The frictional force's magnitude is proportional to the contact surface between blade and vessel and is given by:

$$|\mathbf{F_f}| = (\tau_f\, d)L \tag{5}$$

where L is the blade's length, τ_f is the frictional stress and d the blade depth as shown in Fig. 6.

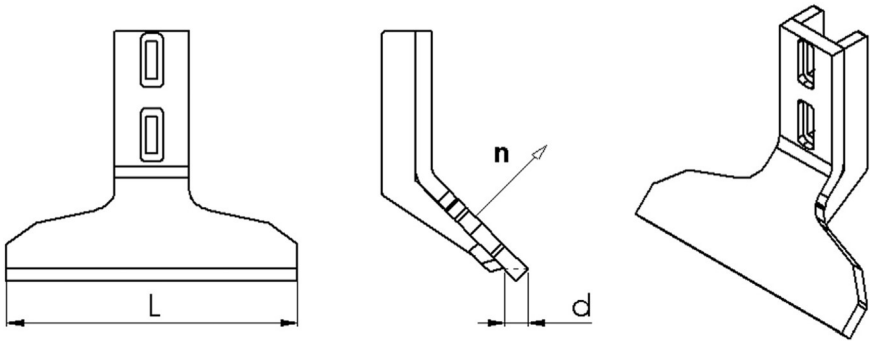

Fig. 6. Blade's geometry.

The viscous force's magnitude is given by:

$$|\mathbf{F_v}| = \mathrm{SL}\mu^* \, \mathbf{n} \cdot \mathbf{v} \tag{6}$$

where S is a viscous coefficient, **n** the normal to the blade surface (see Fig. 6) and **v** the blade velocity [6,19].

In particular, the viscous coefficient S (also called Stokes constant) for blades varies between 2.6 and 4.3. S is 3π for the circumscribed sphere of the blade in an unbound Newtonian fluid. As Cazacliu and Legrand observe in [6], values two to four times lower are reasonable for S, given that the frontal area is significantly lower and the fluid height in the mixer is less than twice the vertical blade height. τ_f results from the strength of coarse aggregates constricted between the vessel wall and the blades. Those parameters have to be fitted onto experimental data. In this paper S and τ_f have not been calculated, as the force's expression is used to qualitatively define the influence of the various geometrical parameters on wear and to reduce their impact.

In planetary movement, the blade velocity can be calculated by:

$$\mathbf{v} = \boldsymbol{\Omega} \times \mathbf{R_G} + \boldsymbol{\omega} \times \mathbf{R_R} \tag{7}$$

where $\boldsymbol{\Omega} \times \mathbf{R_G}$ is the velocity of the gyrational movement and $\boldsymbol{\omega} \times \mathbf{R_R}$ is the velocity in the rotational movement. Radius $\mathbf{R_G}$ is the distance from the center of the planetary gear O to the center of the star O'; radius $\mathbf{R_R}$ is the radius of the star that corresponds to the distance between the center of the star O' and the middle point of the blade front M (see Fig. 2, 3 and Fig. 7). $\boldsymbol{\Omega}$ and $\boldsymbol{\omega}$ are the angular velocities. The frictional force is perpendicular to the trajectory of the motion. The viscous force has the same direction of **v**.

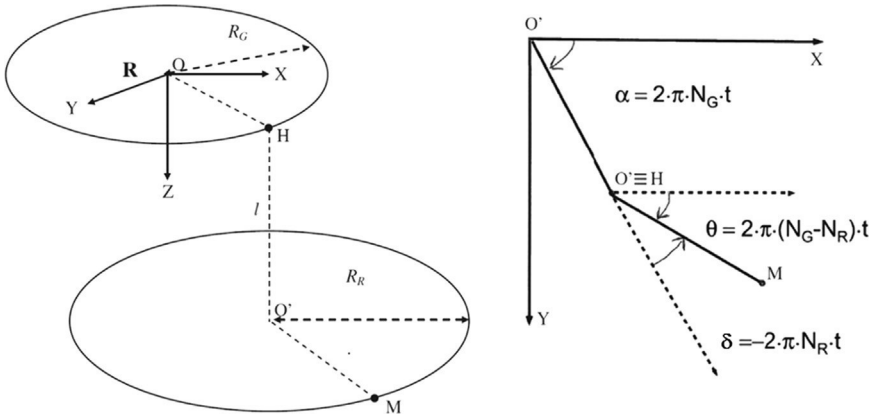

Fig. 7. 3D kinematic scheme for a concrete planetary mixer (left) and its horizontal ($\vec{X} - \vec{Y}$) plane projection (right).

In the studied planetary mixer, the distance between the blades and the tank's bottom is 3 mm, the minimum distance between the blade and the lateral surface of the tank is 65 mm, the blade's depth d (in the bottom plane) is 28 mm.

In addition, the power consumption P is expressed by:

$$P = (\mathbf{F_f} + \mathbf{F_v}) \cdot \mathbf{v} \tag{8}$$

2.2. Blade's kinematics

The blade can be supposed to translate at a constant speed equal to the speed of its central point, calculated in the configuration corresponding to the blade's maximum distance from the tank's center. In that situation, both interaction forces with the fluid and shear rate are at their maximum values, so that wear issues are exalted.

The speed of the central point of the blade is determined by solving a simple kinematic problem, often approached in applications related to mechanical or food engineering [20].

Considering M to be the central point of the blade, the instantaneous position of M in the fixed reference frame R (O; $\vec{X}$; $\vec{Y}$; $\vec{Z}$), in which $\vec{Z}$ is tank symmetry axis, is given by:

$$(\overrightarrow{OM})_R = \overrightarrow{OH} + \overrightarrow{HO'} + \overrightarrow{O'M}. \tag{9}$$

Introducing the following variables and considering gyrational and rotational motions having constant angular speed, the kinematic scheme (Fig. 7) allows determining position and velocity of the point M in the fixed reference frame:

α gyrational angle (rad);

δ rotational angle (rad);

R_G radius of the gyrational motion (m);

R_R radius of the rotational motion (m);

N_G rotational speed of the gyrational motion (rev·s^{-1}, clockwise);

N_R rotational speed of the rotational motion (rev·s^{-1}, counterclockwise).

$$(\overrightarrow{OH})_R = \begin{cases} R_G \cdot \cos(2\pi \cdot N_G \cdot t) \\ R_G \cdot \sin(2\pi \cdot N_G \cdot t) \\ 0 \end{cases} \quad (10)$$

$$(\overrightarrow{HO'})_R = \begin{cases} 0 \\ 0 \\ \overrightarrow{HO'} \end{cases} \quad (11)$$

$$(\overrightarrow{O'M})_R = \begin{cases} R_R \cdot \cos[2\pi \cdot (N_G - N_R) \cdot t] \\ R_R \cdot \sin[2\pi \cdot (N_G - N_R) \cdot t] \\ 0 \end{cases} \quad (12)$$

Therefore, the position of the point M is:

$$(\overrightarrow{OM})_R = \begin{cases} R_G \cdot \cos(2\pi \cdot N_G \cdot t) + R_r \cdot \cos(2\pi(N_G - N_R) \cdot t) \\ R_G \cdot \sin(2\pi \cdot N_G \cdot t) + R_r \cdot \sin(2\pi(N_G - N_R) \cdot t) \\ HO' \end{cases} \quad (13)$$

By simply differentiating the position with respect to the time, the instantaneous velocity vector of the point M is easily obtained:

$$(\vec{v}_M)_R = \left(\frac{d\overrightarrow{OM}}{dt}\right)_R = \begin{cases} -2\pi R_G N_G \cdot \sin(2\pi \cdot N_G \cdot t) - 2\pi R_R (N_G - N_R) \cdot \sin(2\pi(N_G - N_R) \cdot t) \\ 2\pi R_G N_G \cdot \cos(2\pi \cdot N_G \cdot t) + 2\pi R_R (N_G - N_R) \cdot \cos(2\pi(N_G - N_R) \cdot t) \\ 0 \end{cases} \quad (14)$$

Hence, the magnitude of instantaneous velocity of M is given by:

$$\|\vec{v}_M\| = 2\pi\sqrt{(R_G N_G)^2 + R_R^2 (N_R - N_G)^2 - 2R_G R_R N_G (N_R - N_G)\cos(2\pi N_R \cdot t)} \quad (15)$$

2.3. Wear and proposal of a new blade's shape

The standard mixing blades have a "T" shape, with vertical axial symmetry. They are made in Ni-hard iron by casting with a minimum hardness of 550 HB. The mixing operation generates wear mostly on the outer side of the blade. This phenomenon is well displayed in Fig. 8, where a new and a completely worn T blade (after about 6000 cycles working with a standard concrete mix) are shown. The geometry of this part has not a great influence on most of the mixing procedure but it has a fundamental role during the discharge operation.

Fig. 8. Comparison between new (left) and worn (right) blades.

The damage of blades is generally due to three wear mechanisms: abrasive, erosive and corrosive wear. The main phenomena are abrasive and erosive wear, due to mechanical phenomena. Abrasive wear is due to the mechanical contact between the blade and harder solid aggregates in the mixture and it occurs mainly in the dry phase. Erosive wear is due to the mixture slurry flow and thus to the impact of solid or liquid particles against the surface of the blade. Thus, erosive wear is prevalent in the wet phase.

Corrosive wear is mainly a chemical phenomenon depending on the blade's materials and the slurry's chemical composition. Also other mechanical specifications such as fluid pressure on the blade's surfaces, mixture granulometry and blade's kinematics are important parameters.

Steel and cast iron immersed into concrete are subjected to passivation phenomena due to the high alkalinity generated by the cement components' hydration reactions.

In fact, it is well known that the alkalinity of the cement paste stimulates the creation of a passive film of $Fe(OH)_3$ or Fe_2O_3 which protects the steel components from corrosion. Thus, at high pH levels, the corrosion and wear rates decrease.

The pH value of the cement paste is normally greater than 12.5 and some researchers argue that the threshold safety value to prevent corrosion is around 11.5.

So, the passive film is a kind "natural" wear resistant and adherent coating protecting steel from corrosive wear.

Many researchers have worked on this topic, for example Cabrini et al. [21] by means of electrochemical tests and scanning electron microscopy (sem). However, results are very specific and may significantly vary with concrete and steel compositions. This of course depends on the speed and geometry of the blades and the size and hardness of the solid particles of the concrete. In the industrial field it is generally accepted that, due to the mixing speed normally reached in the concrete mixers and the chemical composition of most concretes, corrosive wear is negligible if compared to erosive wear.

Assuming that the mixture/blades interaction forces are not so different in the various phases of the mixing process and roughly considering that the longest is the phase the higher is energy consumption, and consequently the worn volume (classic Reye's hypothesis), our attention was focused on the phases after the water addition and consequently on considering erosive wear.
According to the mathematical models discussed in the previous chapter, blades can be considered as (almost) rigid bodies moving inside a high density Bingham fluid. Moreover, being the blades' velocities generally quite small and the distance between the blades considerable (except in the central area of the planetary mixer, where the blades' velocities are even smaller) we can neglect mutual blades' interactions for wear issues analysis. At the same time, we can consider concrete slurry to be practically still at a certain distance from the blade.
As Cazacliu and Legrand note, the frictional force given by Eq. (5) is considered proportional to the contact surface between blade and vessel and thus it is higher when distance between blade and tank's wall is smaller. In fact, the slurry flow's velocity gradient between the outer portion of the blade's surface and the tank's wall is at its maximum value when the blade occupies the position nearest to the tank's wall. In addition, also the viscous force is at its maximum value when the blade occupies the nearest position to the tank's wall.
This is also the reason why the outer part of the blade's surface is the most interested by wear. According to all these considerations, we propose a modification of the actual "T" shape in a simple way, essentially in its outer part, with the goal of lowering local power consumption and wear. Since the power consumption depends on the scalar product between vectors representing blade/fluid interaction force and blade's velocity (Eq. (8)), we can operate in order to reduce both their moduli but also modifying the angle between the vectors [22,23]. Thus, we proposed the modified geometry of the blade schematically represented in Fig. 9: the outer part of the "standard" T shaped blade has still a straight profile, but bent by an angle β_i with respect to the standard one (Fig. 9). The β_i angle is measured in two different planes: the plane of the blade surface, that is the plane of normal **n** (see Fig. 9c) and the plane perpendicular to the last one (see Fig. 9a). Fig. 9b, d, and e represent the bent blade in the working position, where **n'** is the normal to the bent surface. We cannot provide the full detailed description of the profiles of the new blades because of a non-disclosure agreement with our industrial partners, but the range of β_i we analyzed is from 0° to 50°. Within this range we identified three β_i values of major interest corresponding to three angles β_1, β_2 and β_3, (with $\beta_1<\beta_2<\beta_3$).

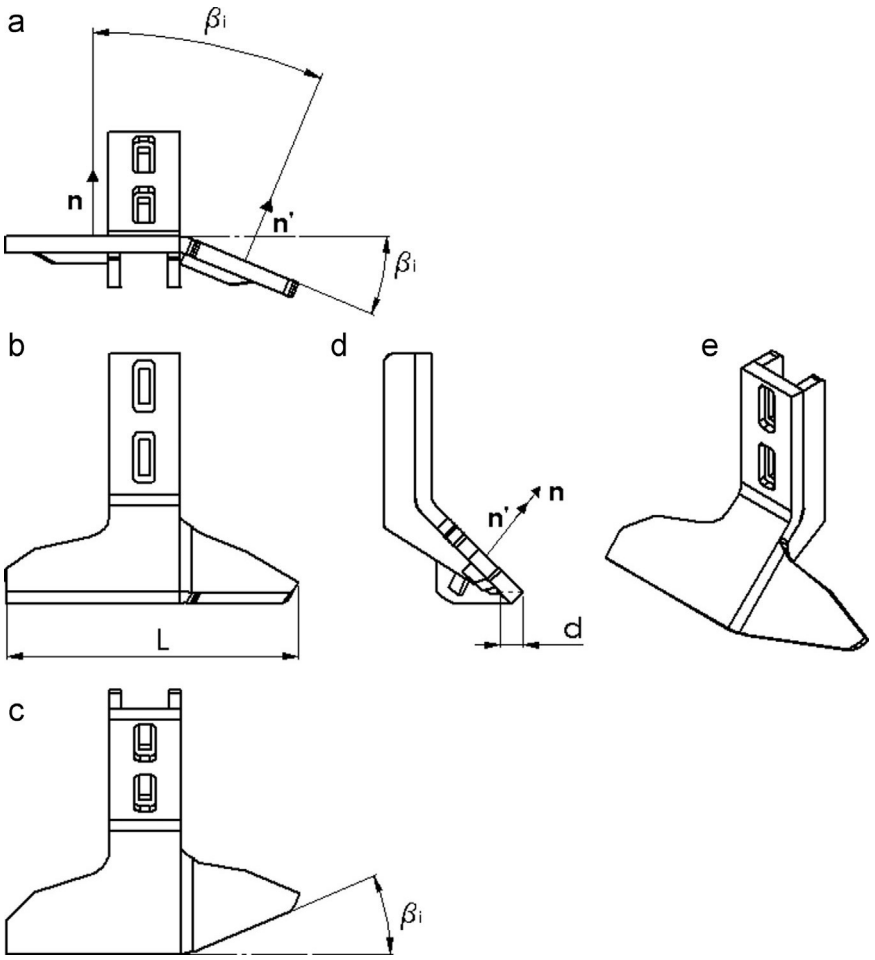

Fig. 9. New blade's main parameters.

The fact that the new design is better in terms of less wear volume was to be expected as the profile of the blade is bent in the same direction of flow so the impact angle is changed.

Also, a kinematic analysis of the new bent blades and of the standard T one has been carried out and the results have been compared. As a result, lower peripheral speeds have been calculated for the bent blades, as their outer edge is closer to the rotation center than the standard T blade's one.

For instance, Fig. 10 shows the velocities of the standard T blade (a) and the proposed new blade bent by a β_3 angle (b) in 5 different points of the front profile. P_M represents the medium point on the blade's profile. From this picture, one can note that points 1 and 2 on the T blade have a maximum velocity higher than the corresponding points 1 and 2 on the bent blade.

Consequently, lower peripheral speed means lower viscous forces and wear.

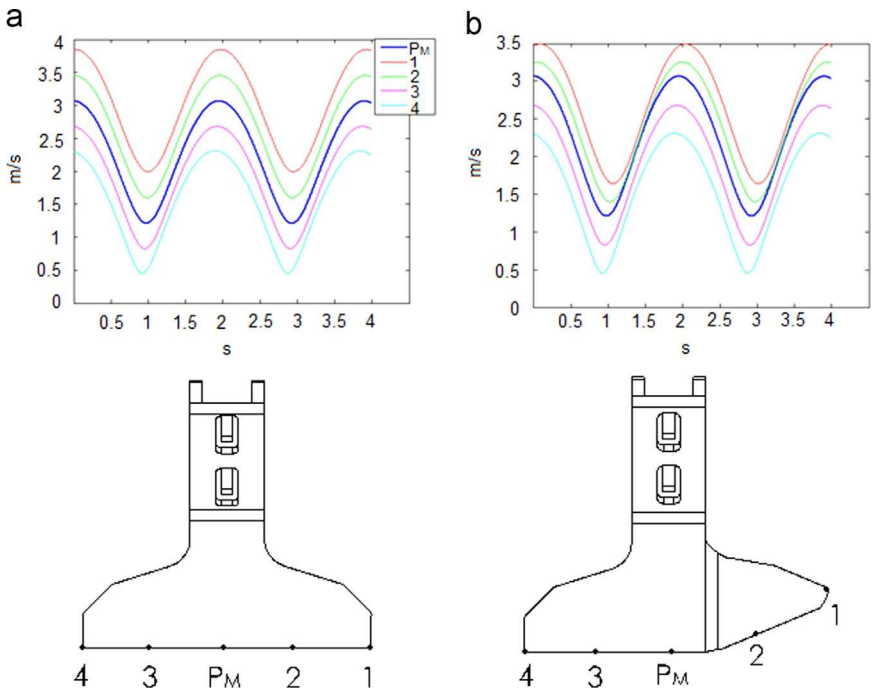

Fig. 10. Speeds of the T blade (a) and the new β_3 blade (b) in 5 points of the front profile.

3. Experimental tests and 2D validation

3.1. Experimental setup

The purpose of this research phase was to perform experimental tests in order to:

- Verify the wear resistance of the new blade's profiles and choose the best design angle (β_1, β_2 or β_3);
- Evaluate the wear rate of the chosen new blade's profile with respect to the standard T blade.

For those purposes, we realized some prototypal blade sets in structural steel (Fe360 – S235) to be tested during exercise in two stars planetary concrete mixers (MP1500) available at a company whose market field extends in manufacturing of concrete products for civil, roads, railways and other industrial applications. The material was chosen instead of the standard Ni-hard cast iron in order to achieve wear in a short time during tests.

The mixture composition during the tests was characterized by the following specifications: cement 675 kg ±3%, water 270 l ±3%, sand and gravel 2680 kg ±3%, additives 5 kg ±5%, humidity 14.5%, water/powder 0.4l/kg.

3.2. Comparison of bent blades and choice of the best β angle

In order to evaluate the wear rates of the three new shaped blades, six new blades have been assembled in a two stars planetary concrete mixer (two β_1, two β_2 and two β_3 blades), according to the configuration showed in Fig. 11.

The blades have worked for a certain time (3000 cycles), up to wear.

The choice to mount the six blades in the same mixer assured the same working time and the same operating conditions with the same mixture composition.

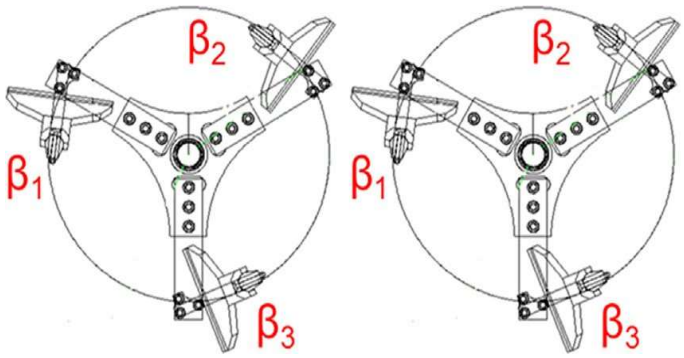

Fig. 11. Experimental setup for the comparison of the bent blades.

In principle, the blades can be compared on the basis of their worn 2D profiles. This comparison allows choosing the best design angle among those tested.

Using the experimental setup shown in Fig. 11, we made the mixer work with different mixtures following the normal mixing cycle. Periodically the mixer was emptied, cleaned and the blade's profiles were monitored throughout a very simple 2D image processing technique. We were then able to analyze the profiles' changes over time for the various blades in reason of the increasing wear. In order to better assess the performance of the blades depending on their different geometries, we evaluated multiple parameters describing the wear progress over time.

A first indication of the wear progress is the reduction of the length of the straight part of the blade's profile. Then we assessed the overall reduction of the blades' profile length (sum of straight and bent parts of the profile). Finally, we have identified 5 points (P1-P5) inside the profiles and there we measured the reduction of the blade's thickness over time.

All those parameters and therefore the wear progress were measured on the new (not worn) blades, and on the worn ones after each of the three series of mixing cycles of our experimental program, whose total duration was indicated as t_1, t_2 and t_3.

The worn profiles of each blade have been projected on a horizontal plane and displayed on a graph at the end of every observation period.

By analyzing the graphs obtained in such a way, the magnitude of the wear progress over time can be easily verified. For example, in Fig. 12 we can observe the evolution of the profile of the β_1 bent blade during the wear progress over time.

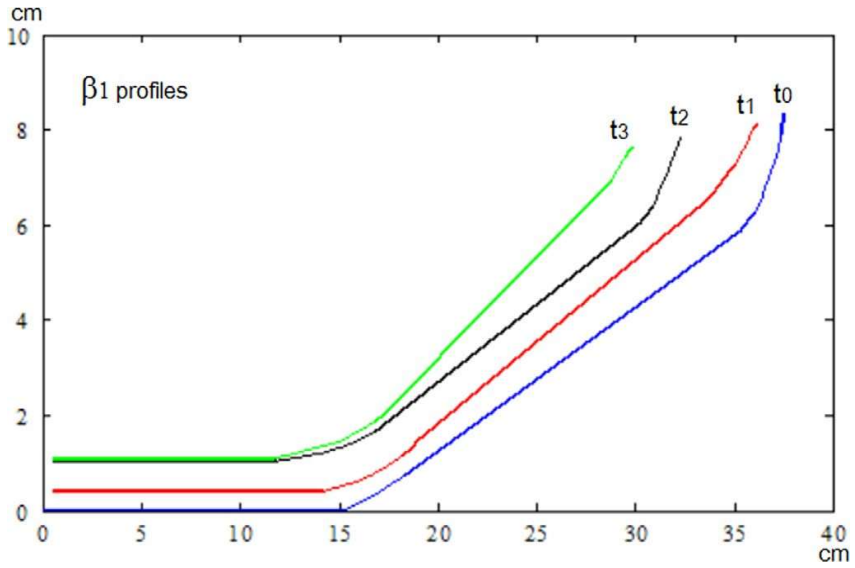

Fig. 12. Front profile of β_1 bent blade during wear progress.

The results of the comparative analysis of the profiles of bent blades at the end of the whole test (time t_3) are shown in Fig. 13. For each profile, the remaining length of the straight part was measured: it seems quite clear that the blade bent by the angle β_3 is the most resistant to wear.

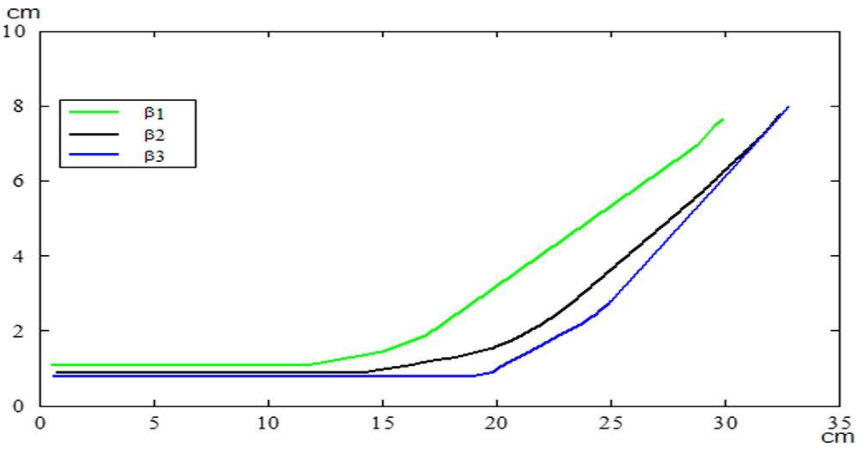

Fig. 13. Comparison among the profiles of the three bent blades at the end of the experimental tests (time t_3).

Analyzing a bit deeper the same experimental results, the overall length of the blade profile was measured as a function of time. In particular, we estimated the percentage of the total worn blade's length at the end of the test through the simple formula:

$$\% L_w = \frac{L_{new} - L_{t_3}}{L_{new}} \% \quad (16)$$

where L_{new} is the length of the non-worn blade, L_{t_3} is the length of the worn blade after the time t_3. All the obtained results are summarized in Table 1, where the length indicated into the table is the average of the two tested blades in the first experiment. We have observed that the results corresponding to two equal blades are similar.

Table 1. Results of comparison of wear for the three bent blades in terms of length

Bent blade angle	Blade's total length (mm)				Blade's length percentage reduction after t3 (%)
	New	after 1st period t_1	after 2nd period t_2	after 3rd period t_3	
β_1	400	370	332	307	-23.3%
β_2	400	385	360	336	-16.0%
β_3	400	386	361	342	-14.5%

The bent blade with the widest angle (β_3) has resulted to be the best in terms of wear rate calculated with Eq. (16), with a reduction in length of about 14.5% against the value almost doubled (23.3%) of the blade with the narrowest angle (β_1).

Finally, we identified five characteristic points on the different profiles of the bent blades, indicated as P_1, P_2, P_3, P_4 and P_5. In correspondence of these points, the thickness of the non-worn blade and of the blade at the end of each time period t_1, t_2, t_3 was measured. Then, through a simple difference, the thickness of the worn material was determined and the results were displayed in graphs. For example, Fig. 14 displays the thicknesses of the worn material after the whole test (time period t_3) as a function of the position inside the blade (measuring points P_1, P_2, P_3, P_4 and P_5).

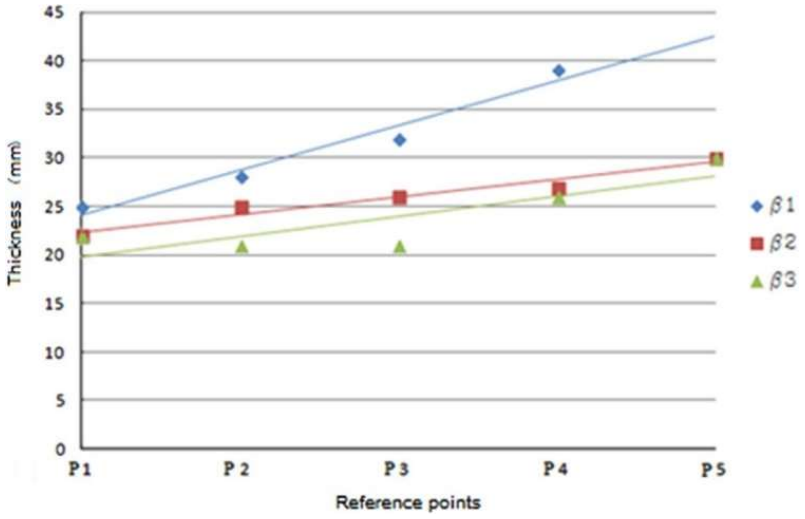

Fig. 14. Thicknesses of the worn material after the time t_3.

Even from those results, the blade bent by the angle β_3 appears as the most wear resistant because the worn thicknesses are smaller if compared to other geometries.
From the analysis of every parameter taken into account during this experimental campaign, the blade bent by the angle β_3 has clearly proven to be the best among all in terms of wear rates [24].

3.3. Comparison of bent blades vs standard "T" blades.

After choosing the blade bent by the angle β_3 as the best one among the tested geometries, we performed a second experimental campaign by using the setup shown in Fig. 15. Three "T" blades and three new shaped blades bent by an angle β_3 were assembled in a two stars planetary concrete mixer and worked for a certain time, up to wear. The choice to mount the six blades in the same mixer assured the same working time and the same service conditions with the same mixture composition.

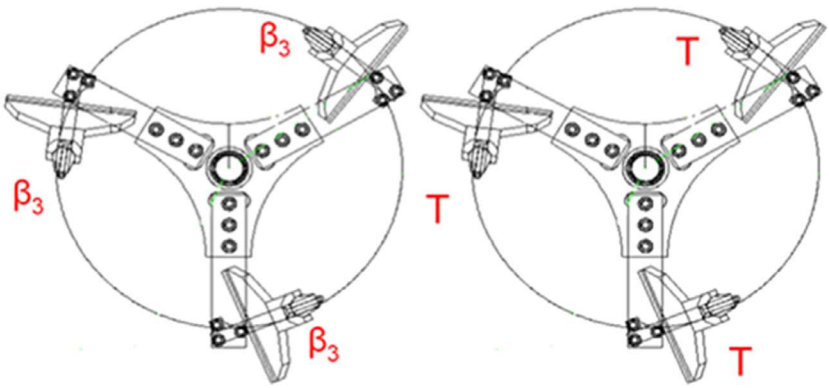

Fig. 15. Thicknesses of the worn material after the time t_3.

The aim of this second experimental campaign was to perform a detailed direct comparison between the standard T blades and the new shaped blades in terms of wear resistance.

Also in this test, we performed three series of mixing cycles, whose total durations were indicated as t_1, t_2 and t_3.

We measured the profiles of the two types of blade at each time period t_1, t_2 and t_3. This procedure allowed us to check the wear progress over time on the two types of profile simultaneously, in order to achieve a direct comparison.

Fig. 16 shows the evolution of the bent blade's profile over time periods t_1, t_2 and t_3, while Fig. 17 displays the evolution of the standard T blade's profile over time periods t_1, t_2 and t_3.

As in this case the blades' profiles are significantly different, we chose a different comparison parameter for assessing their wear resistance. In fact, we analyzed the whole profile and not just the front profile of the blades (that is directly invested by the mixture, and therefore the most interested by wear).

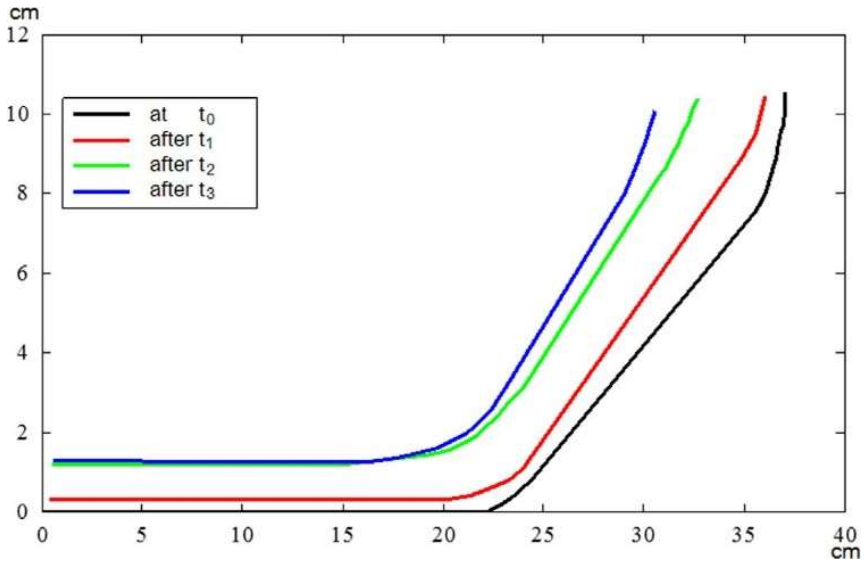

Fig. 16. Comparison among new and worn profiles of the β_3 bent blade after the three working periods.

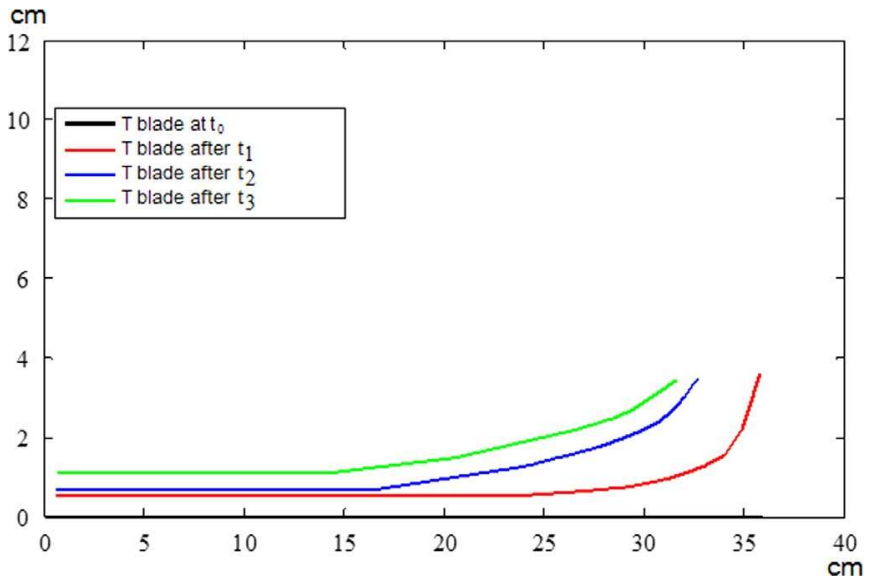

Fig. 17. Comparison among new and worn profiles of the standard T blade after the three working periods.

For each kind of blade, the profile on the horizontal plane (at a certain distance from the vessel floor) are obviously closed curves: the area of these curves was measured in order to evaluate, by a simple difference, the wear rate over time.

These 2D measurements are not exactly related to the worn volume (classical Reye's law) because the height (in the vertical direction) of the blade is not completely homogeneous.

Nevertheless, in this evaluation we refer to the area of the blade's profile as 'volume per unit thickness', because we assume that the variations of area per unit height are quite limited.

We will overcome this rough assumption by performing 3D evaluations of the worn volumes by means of 3D metrological instruments. However, for the purpose of this paper a 2D comparison is pretty enough since the goal is not to quantify the real wear rates but just to assess if the new shaped blade is more wear resistant than the standard T shaped one.

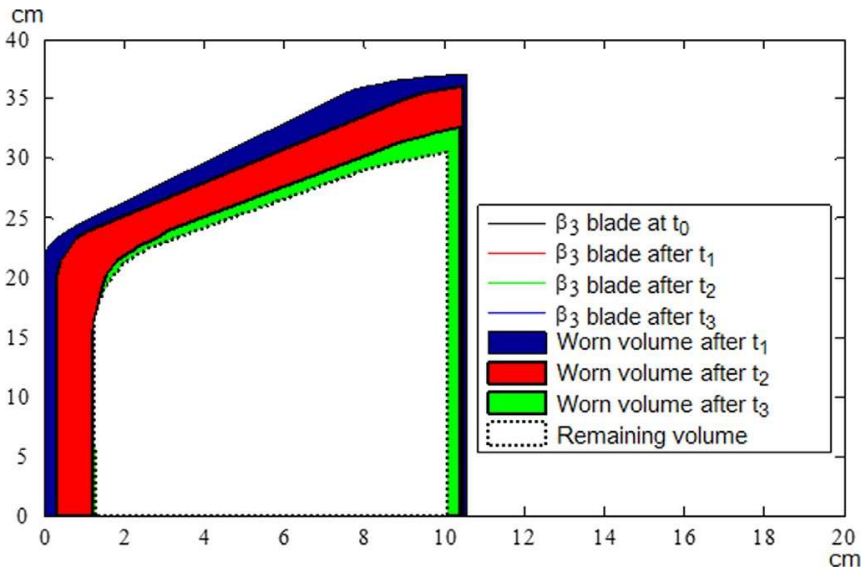

Fig. 18. Worn volume for the bent blade's profile during the three working periods.

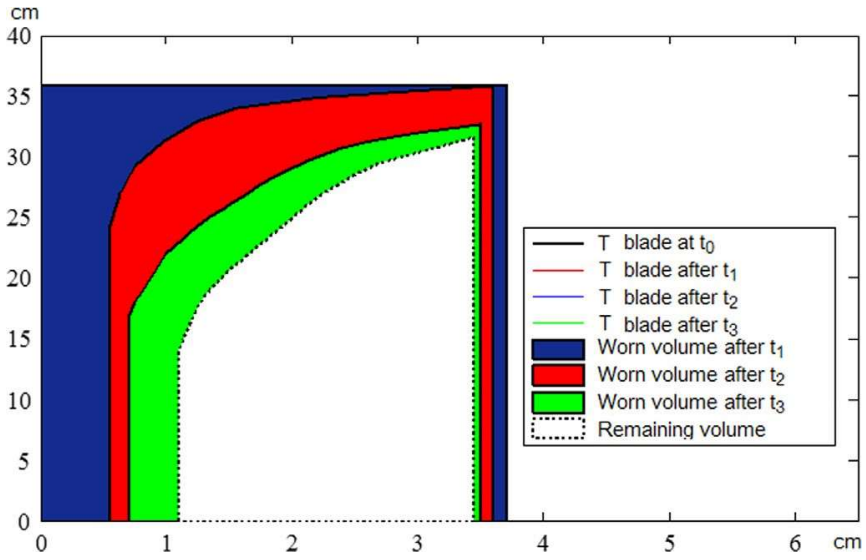

Fig. 19. Worn volume for the standard T blade's profile during the three working periods.

Fig. 18 shows the results of measurements of worn areas for the bent blade's profile during the three working periods and Fig. 19 shows the results of measurements of worn areas for the standard T blade's profile during the three working periods. In these figures, the profiles have been rotated and flipped with respect to those shown in Fig. 16 and Fig. 17.

Blue, red and green areas represents the worn volumes after the various working periods, while the white area represents the remaining volume at the end of the whole experimental test.

The analysis of Fig. 16 to Fig. 19 reveals distinct periods of wear, during tests. Regarding the standard T blade, the first period is characterized by a sharp increase of the wear rate. This is

associated with intense micro-cutting and scratching by the moving abrasive mixtures, which undergo plastic deformation. The same period is not characterized by the same high wear rate for the bent blade. That is to be expected as the profile of the blade is bent in the same direction of the flow, so the impact angle is bigger. After the first period, the wear rate for the T blade keeps on decreasing up to the end of the test. On the contrary, for the bent blade the wear rate increases up to t2 and then it starts decreasing. The length of the period of wear rate increase for the bent blade depends on the wear resistance of the material used for the blades and the level of polish of their working surfaces. Erosion of the surfaces is expressed as subsequent polishing and impact-abrasive wear. With wear of the blades' working edges, the radial gap between the blades and the chamber lining increases. Consequently, the wear rate gradually rises. In the third period, the effects mentioned about the first and the second periods balance each other out.

Table 2 reports the wear rates calculated according to the 2D comparison. The formula used to calculate the wear rate is:

$$\%\, A_w = \frac{A_{new} - A_{t_3}}{A_{new}}\ \%$$

where A_{new} is the area of the non-worn blade in the horizontal plane, A_{t_3} is the remaining area after the time t_3.

Table 2. Results of comparison of wear for the bent blade and the T blade in terms of worn areas in the horizontal plane.

Bent blade angle	Blade's areas (cm^2)					Total wear rate (%)
	Non-worn Area	Worn area after t_1	Worn area after t_2	Worn area after t_3	Remaining area	
β_3 shape	331	28	53	20	230	-30.5%
T shape	132	29	24	18	61	-53.8%

The β_3 bent blade has resulted to be the best in terms of wear rate calculated with Eq. (17), with a wear rate of about 30.5% against the 53.8% of the T blade.

As we have already mentioned this evaluation is not aimed to quantify the real wear rates but just to assess if the new shaped blade is more wear resistant than the standard T shaped one.

The estimation of the wear through weight variation is a very hard issue for two main reasons:

- this estimation during the experimental stages implies thedismount of the blades from the mixing arms. Thus, the adjustment and regulation of the blades' right position would be lost and it would not be possible to set it again, since the initial geometrical references are lost, due to the progressive wear phenomena;

- to estimate wear volumes through weight variation, bladesshould be completely cleaned from concrete. This is almost impossible, since the concrete adheres and harden on the blades and in particular in the attack zone, with risk of damage of the blades or of the mixing arms in case of cleaning and dismounting.

However, the real wear rates and worn volumes will be assessed by means of 3D metrological instruments.

During the tests, no comparative evaluations of the power consumption at the regime phase could be done because the tests were carried out in a production plant and not in a laboratory. In fact, in this production plant the regulation of the mixture slump is done manually by adding water until the power consumption stabilizes at a certain constant value, during the regime phase. For this reason, we evaluated the power consumption with the new blade just before the first water introduction (point 5 in Fig. 5). We have noted a reduction of the power consumption peak of about 2% with the new blade shape.

4. Conclusions

In this paper, we showed and discussed an improved geometry of mixing blades for planetary concrete mixers in terms of wear resistance. In particular, we proposed a new blade's design on the basis of a theoretical qualitative approach (fresh concrete model, actions on the blades, power consumption) an then we performed experimental campaigns in order to study and demonstrate the efficiency of the new blade's geometry. A first experimental campaign was aimed to choose the best geometrical parameters for the new design (β angle) and a second experimental campaign was performed in order to measure the wear rates of the standard

T blades and of the new designed ones. Experimental results, based on a 2D comparison of worn profiles, show that the blade bent by an angle β_3 was the best one in terms of wear resistance if compared with the blades bent by angles β_1 and β_2.

Furthermore, the new blade bent by the angle β_3 shows a better wear resistance and lower power consumption if compared to the standard T blade normally used in planetary concrete mixers.

The goal of the 2D evaluations proposed in this paper was not to quantify the real wear rates of the blades but just to estimate the differences and to assess which of the new shaped blades was the best in terms of wear resistance and if the new design allowed for lower wear rates and longer durability.

Acknowledgments

Authors warmly acknowledge the company S.I.CO.MA. srl – Ponte Valleceppi – Perugia, Italy and Cancellotti srl – Ponte Valleceppi – Perugia, Italy and their whole staffs for providing the blades, the equipment and the planetary concrete mixers used in this work and for their cooperation in gathering data from experimental tests. Special tanks to Mr. Paolo Galletti (S.I.CO.MA. srl CEO) and Ing. Ilaria Gasperini (S.I.CO.MA. srl) for their technical support and Ing. Marco Contini (Cancellotti srl).

References

[1] Ferraris CF. Concrete mixing methods and concrete mixers: state of the art. J Res Natl Inst Stand Technol 2001;106(2):391–9.

[2] Dils J, De Schutter G, Boel V. Influence of mixing procedure and mixer type on fresh and hardened properties of concrete: a review. Mater Struct 2012;45:1673–83.

[3] Rinchi M, Valigi MC, Caputo S. Behavior simulation of a concrete mixture in a turbine pan mixer. Betonw Fertigtl-Tech (Concr Plant Precast Technol) 2015;5:44–51.

[4] Charronnat Y, Beitzel H. Report: efficiency of concrete mixers towards qualification of mixers. Mater Struct 1997;30(1):28–32.

[5] Cazacliu B, Roquet N. Concrete mixing kinetics by means of power measuremet. Cem Concr Res 2009;39(3):182–94.

[6] Cazacliu B, Legrand J. Characterization of the granular-to-fluid state process during mixing by power evolution in a planetary concrete mixer. Chem Eng Sci 2008;63(18):4617–30.

[7] Cazacliu B. In-mixer measurements for describing mixture evolution during concrete mixing. Chem Eng Res Des 2008;86(12):1423–33.

[8] Braccesi C, Landi L. An analytical model for force estimation on arms of concrete mixers. In: proceedings of the ASME international design engineering technical conferences and computer and information in engineering conference 2009, DETC 2009, San Diego, CA (US), 2010.

[9] Terzaghi K, Peck RB. Soil mechanics in engineering practice. III ed.. New York, US: John Wiley and sons Inc; 1996.

[10] Hu C, De Larrard F. The rheology of fresh high-performance concrete. Cem Concr Res 1996;2:283–94.

[11] De Larrad F, Ferraris CF, Sedran T. Fresh concrete: a Herschel-Bulkley material. Mater Struct 1998;31:494–8.

[12] Gram A, Silfwerbrand J, Lagerblad B. Obtaining rheological parameters from flow test-analytical, computational and lab test approach. Cem Concr Res 2014;63:29–34.

[13] Valigi MC, Gasperini I. Planetary vertical concrete mixers: simulation and predicting useful life in steady states and in perturbed conditions. Simul Model Pract Theory 2007;15(10):1211–23.

[14] Valigi MC, Gasperini I. Model-based method predicting useful life of concrete mixers [Modellgestütztes Verfahren zur Vorhersage der Nutzungsdauer von Betonmischern]. Betonw Fertigtl-Tech (Concr Plant Precast Technol) 2005;71 (11):38–42.

[15] Yao Y, Feng Z, Chen S. Strength of concrete reinforced using double-blade mixer. Mag Concr Res 2013;65(13):787–92.

[16] Ferraris CF. Measurement of the rheological properties of high performance concrete: state of the art report. J Res Natl Inst Stand Technol 1999;104 (5):461–78.

[17] Chapkov AD, Bair S, Cann P, Lubrecht AA. Film thickness in point contacts under generalized newtonian EHL conditions: numerical and experimental analysis. Tribol Int 2007;40:1474–8.

[18] de la Guerra Ochoa E, Echavarri Otero J, Sanchez Lopez A, Chacon Tanarro E. Film thickness predictions for line contact using a new Reynolds-Carreau equation. Tribol Int 2015;82(A):133–41.

[19] Valigi MC, Fabi L, Gasperini I. Wear resistance of new blade for planetary concrete mixer. In: Proceedings of the 5th world tribology congress, WTC 2013, Torino (IT), 2013.

[20] Delaplace G, Coppenolle P, Cheio J, Ducept F. Influence of whip speed ratios on the inclusion of air into a backery foam produced with a planetary mixer device. J Food Eng 2012;108:532–40.

[21] Cabrini M, Cortellini M, Lorenzi S, Marcassoli P, Pastore T. Meccanismi di erosione dell'acciaio a contatto con calcestruzzo fresco. Metall Ital 2010;5:39–44.

[22] Valigi MC, Gasperini I. A study on the wear of planetary concrete mixers. Extending the usable-life of mixing blades. CPI-Concr Plant Int 2012;1:50–5.

[23] Valigi MC, Logozzo S, Gasperini I. Study of wear of planetary concrete mixer blades using a 3d optical scanner. In: Proceedings of the international mechanical engineering congress & exposition IMECE 2015, Houston, Texas, US, November 13–19, 2015.

[24] Galletti P. Mixing Blade. Patent WO2014170827A1, 15 April 2014.